Available online at www.sciencedirect.com

ScienceDirect

Procedia CIRP 82 (2019) 503–508

www.elsevier.com/locate/procedia

17th CIRP Conference on Modelling of Machining Operations

Effect of axial vibrations on regenerative chatter in robotic milling

Yaser Mohammadi[a], Keivan Ahmadi[a,*]

[a]*Department of Mechanical Engineering, University of Victoria, Victoria, British Columbia V8W 2Y2, Canada*

Abstract

The highly flexible structure of industrial robots introduces new challenges to modeling vibrations during robotic milling processes. This paper studies the contribution of the axial vibrations of the milling end-effector to regenerative chatter in robotic milling. While axial vibrations of the tool are usually neglected in standard CNC machines, in industrial robots, they may significantly affect the stability of the process. The numerical case studies in this work show that the modulation of the nominal depth of cut due to axial vibrations may cause nonlinearities in the cutting forces. In addition, it is also shown that axial vibrations may cause the feed-generated and edge forces to affect the stability of regenerative vibrations in robotic milling.

Peer-review under responsibility of the scientific committee of The 17th CIRP Conference on Modelling of Machining Operations

Keywords: Robot; Machining; Milling; Dynamics; Chatter; Vibration; Stability; Removal rate

1. Introduction

Compared to traditional CNC machine tools, industrial robots offer a larger workspace and higher versatility at a lower price. These advantages of robots are undermined by their higher structural flexibility causing excessive static deflections and structural vibrations during machining applications [1, 2, 3, 4].

The primary focus of the vibration modeling research in robotic milling has been on adopting the chatter analysis methods that are commonly used for traditional machining systems [5]. Wang et al. [6] showed that mode coupling mechanism, caused by flexible low frequency modes of the robot structure, is the dominant source of vibrations in robotic milling. They applied the method developed by Gasparetto [7] to obtain a criteria for mode coupling chatter stability based on principal stiffness values and directions of the robot. Cen et al. [8] presented a mode coupling chatter avoidance technique by considering the conservative congruence transformation (CCT) for mapping of stiffness matrices between joint and Cartesian spaces. They showed that the principal stiffness directions of the robot can vary by changing the end-effector feedrate; hence, the process can be stabilized through controlling the feedrate. Huynh et al. [9] developed a Multi-Body Dynamic (MBD) model of an articulated robot which was then used in a numerical milling simulation environment to predict stability limits. Mousavi et al. [10] developed a MBD model of robot using beam elements as flexible links. Then, they obtained the stability diagrams through the frequency domain regenerative chatter analysis method developed by Budak and Altintas [11]. It should be noted that this chatter analysis method inherently covers both mode coupling as well as the regenerative chatter mechanisms [12].

The complex structural dynamics of articulated robotic manipulators, compared to traditional machine tools, calls for major modifications to the existing chatter analysis methods. Cordes et al. [13] showed that the strong coupling between the dynamics of the articulated robotic arm in feed, normal, and axial directions must be considered in modeling chatter in robotic milling. Such coupling is usually neglected in conventional machine tools. They also showed a strong non-symmetry in the Frequency Response Functions (FRF) matrix, which is not observed in machine tools. In this paper, we highlight another influential feature in robotic machining which is usually neglected in conventional machine tools. Although the dynamic deflections of the tool in the axial direction was considered in [13], its effect on the modulation of the axial depth of cut was neglected. In this work, chatter in robotic milling is modelled by considering the modulation of the nominal axial depth of cut due to the vibrations in the axial direction. The numerical examples presented in this work show that the modulation of nominal axial depth of cut results in the feed and edge forces altering

* Corresponding author. Tel.: +1-250-721-8694 ; fax: +1-250-721-6051.
E-mail address: kvahmadi@uvic.ca (Keivan Ahmadi).

2212-8271
Peer-review under responsibility of the scientific committee of The 17th CIRP Conference on Modelling of Machining Operations
10.1016/j.procir.2019.04.235

the stability of vibrations. Also the modulation of nominal axial depth of cut leads to nonlinearities in the cutting forces, which affects the stability of vibrations as well.

2. Milling forces model

A Multi-Degree-Of-Freedom (MDOF) milling system with a round-end tool (e.g. ball end or bull nose) having N teeth is considered as shown in Fig. 1 . Assuming a small axial depth of cut, a, in robotic milling, the cutting forces on each tooth j ($j = 1, ..., N$) are assumed to be concentrated at the midpoint of its engaged length. The forces acting on each tooth are functions of axial depth of cut a, and chip thickness h_j. The total chip thickness consists of the portion generated by feed motion of the tool, $h_{f,j}$, and the portion generated by the vibrations of the tool, $h_{v,j}$ [12]:

$$\begin{aligned} h_j(\varphi_j) &= h_{f,j}(\varphi_j) + h_{v,j}(\varphi_j); \\ h_{f,j}(\varphi_j) &= f_t \sin\varphi_j \sin\gamma \\ h_{v,j}(\varphi_j) &= \Delta x \sin\varphi_j \sin\gamma + \Delta y \cos\varphi_j \sin\gamma - \Delta z \cos\gamma \end{aligned} \tag{1}$$

where f_t is the feed per tooth, $\varphi_j = (j-1)\frac{2\pi}{N} + \Omega t$ is the instantaneous immersion angle of tooth j at the spindle speed Ω, and $\Delta x = x(t) - x(t-\tau)$, $\Delta y = y(t) - y(t-\tau)$ and $\Delta z = z(t) - z(t-\tau)$ are the regeneration terms with the tooth passing period $\tau = \frac{2\pi}{N\Omega}$. The milling forces in tangential, radial and axial directions acting on tooth j can be obtained as follows [12]:

$$\begin{aligned} F_{t,j}(t) &= K_{te}\, s + K_{tc} h_j(\varphi_j) a \\ F_{r,j}(t) &= K_{re}\, s + K_{rc} h_j(\varphi_j) a \\ F_{a,j}(t) &= K_{ae}\, s + K_{ac} h_j(\varphi_j) a \end{aligned} \tag{2}$$

where $s = \frac{a}{\sin\gamma}$, and γ is the cutting edge angle at the midpoint of the axial engagement, as shown in Fig. 1. The constants, $K_{mn}, m = t, r, a; n = e, c$, represnt the edge and cutting force coefficients [12] .The total forces in Cartesian coordinates are obtained by adding the contribution of the cutting forces generated by each one of the N flutes:

$$\begin{aligned} \mathbf{F}(t) &= \begin{bmatrix} F_x & F_y & F_z \end{bmatrix}^T \\ &= \sum_{j=1}^{N} \mathbf{R}(\varphi_j) g(\varphi_j) \begin{bmatrix} F_{t,j}(t) & F_{r,j}(t) & F_{a,j}(t) \end{bmatrix}^T \end{aligned} \tag{3}$$

$$g(\varphi_j) = H(\varphi_j - \varphi_{st}) - H(\varphi_j - \varphi_{ex})$$

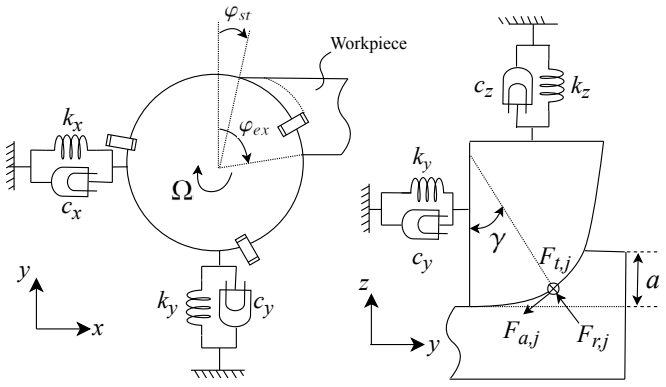

Fig. 1. Three dimensional milling forces model.

In Eq. 3, H is a unit step function and $g(\varphi_j)$ is a Heaviside function that determines if tooth j is engaged with the workpiece. The start and exit angles, φ_{st} and φ_{ex}, respectively, are illustrated in Fig. 1. Matrix $\mathbf{R}(\varphi_j)$ projects the tangential, radial, and axial forces on the x, y, and z directions:

$$\mathbf{R}(\varphi_j) = \begin{bmatrix} -\cos\varphi_j & -\sin\varphi_j \sin\gamma & -\sin\varphi_j \cos\gamma \\ \sin\varphi_j & -\cos\varphi_j \sin\gamma & -\cos\varphi_j \cos\gamma \\ 0 & \cos\gamma & -\sin\gamma \end{bmatrix} \tag{4}$$

In machining with conventional machine tools, the system is much more stiff in axial direction compared to lateral directions; hence, the axial depth of cut is assumed to be constant $a = a_o$. However, in robotic machining systems, the structure in axial direction can be as flexible as the lateral directions; or even more flexible depending on the robot posture. Therefore, axial vibrations become significant and cause the actual depth of cut to vary. In this paper, the actual depth of cut is assumed to be modulated by the axial vibration:

$$a(t) = a_o - z(t) \tag{5}$$

Substituting $a(t)$ and h_j from Eqs. 5 and 1, respectively, in Eq. 2, and then the resulting tangential, radial, and axial force components in Eq. 3, leads to the following expression of the total cutting forces applied on the milling tool:

$$\begin{aligned} \mathbf{F}(t) &= \mathbf{F}_e(t) + \mathbf{F}_f(t) + \mathbf{F}_r(t); \\ \mathbf{F}_e(t) &= \sum_{j=1}^{N} \mathbf{R}(\varphi_j) g(\varphi_j) \begin{bmatrix} K_{te} & K_{re} & K_{ae} \end{bmatrix}^T (a_o - z) / \sin\gamma \\ \mathbf{F}_f(t) &= \sum_{j=1}^{N} \mathbf{R}(\varphi_j) g(\varphi_j) \begin{bmatrix} K_{tc} & K_{rc} & K_{ac} \end{bmatrix}^T \sin\varphi_j \sin\gamma \\ &\qquad f_t (a_o - z) \\ \mathbf{F}_r(t) &= \sum_{j=1}^{N} \mathbf{R}(\varphi_j) g(\varphi_j) \begin{bmatrix} K_{tc} & K_{rc} & K_{ac} \end{bmatrix}^T \sin\gamma \\ &\qquad \left(\Delta x \sin\varphi_j + \Delta y \cos\varphi_j - \Delta z \cot\gamma\right)(a_o - z) \end{aligned} \tag{6}$$

As shown in Eq. 6, the total milling forces, $\mathbf{F}$, consist of the forces generated by the feedrate $\mathbf{F}_f$ (will be referred to as feed forces in this paper), edge forces $\mathbf{F}_e$ and regenerative forces $\mathbf{F}_r$. In conventional machine tools, due to their high stiffness in axial direction, depth of cut is assumed to be constant at a_o and thus the terms that depend on the axial deflection (z) are disappeared from Eq. 6. As a result, the edge and feed forces do not influence the stability of the system and are neglected in chatter analysis. In robotic milling, as shown in Eq. 6, the modulation of depth of cut results in new displacement dependent terms in the edge and feed forces, and a nonlinear term in the regenerative force. In the following two sections, the effect of these additional components on the stability of vibrations will be studied.

3. Effect of feed and edge forces

The existing chatter stability prediction methods, such as the frequency domain solution [11] and the time domain semidiscretization method [14], are applied to linear milling systems. As it was shown in the previous section, the dynamic feed and

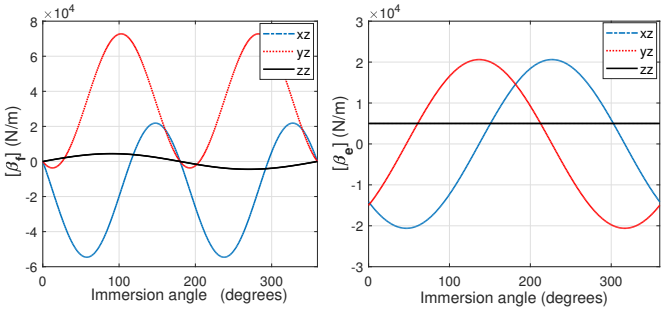

Fig. 2. Variation of the additional coefficients $[\beta_e]$ and $\lfloor\beta_f\rfloor$ with rotation of cutting tool.

edge forces are linear functions of axial vibrations (Eq. 6). Hence, by ignoring the nonlinear term of the regenerative forces, the effect of dynamic feed and edge forces on stability of the system can be investigated through the existing linear methods. In this section, Zero Order Approximation (ZOA) method is used to determine the stability limit of the system considering the effect of axial vibrations on feed and edge forces.

3.1. Stability lobe diagrams

As shown in Eq. 6, the feed and edge forces consist of a term that depends on the nominal depth a_o, and another term that depends on axial vibrations $z(t)$. While the former term does not affect the stability of the system [12, 11] and can be dropped from equations, the latter terms must be considered in the stability analysis. Also, the nonlinear terms in the regenerative component of the forces are neglected in this section. As a result, the total milling forces in Eq. 3 can be re-written as follows:

$$\mathbf{F}(t) = a_o\,[\alpha]\,(\mathbf{X} - \mathbf{X}^\tau) - \left([\beta_e] + \lfloor\beta_f\rfloor\right)\mathbf{X} \tag{7}$$

where $[\alpha]$ is the directional coefficient as given in [11] and the non-zero elements of $[\beta_e]$ and $\lfloor\beta_f\rfloor$ are as follows:

$$\beta_{e,xz} = \sum_{j=1}^{N} g(\varphi_j)\left(-K_{te}\cos\varphi_j - (K_{re}\sin\gamma + K_{ae}\cos\gamma)\sin\varphi_j\right)/\sin\gamma$$

$$\beta_{e,yz} = \sum_{j=1}^{N} g(\varphi_j)\left(K_{te}\sin\varphi_j - (K_{re}\sin\gamma + K_{ae}\cos\gamma)\cos\varphi_j\right)/\sin\gamma$$

$$\beta_{e,zz} = \sum_{j=1}^{N} g(\varphi_j)\,(K_{re}\cos\gamma - K_{ae}\sin\gamma)/\sin\gamma$$

$$\beta_{f,xz} = \sum_{j=1}^{N} g(\varphi_j)\left(-K_{tc}\sin\varphi_j\cos\varphi_j - (K_{rc}\sin\gamma + K_{ac}\cos\gamma)\sin^2\varphi_j\right)f_t\sin\gamma$$

$$\beta_{f,yz} = \sum_{j=1}^{N} g(\varphi_j)\left(K_{tc}\sin^2\varphi_j - (K_{rc}\sin\gamma + K_{ac}\cos\gamma)\sin\varphi_j\cos\varphi_j\right)f_t\sin\gamma$$

$$\beta_{f,zz} = \sum_{j=1}^{N} g(\varphi_j)\,(K_{rc}\cos\gamma - K_{ac}\sin\gamma)\,f_t\sin\varphi_j\sin\gamma$$

Figure 2 shows the variation of the additional coefficients $[\beta_e]$ and $\lfloor\beta_f\rfloor$ with the immersion angle. Similar to directional coefficients $[\alpha]$, they vary periodically with the rotation of the cutting tool; hence, they can be expressed as Fourier series. Following the ZOA method, the average term of the Fourier series is used for stability analysis [11]:

$$[A_0] = \frac{1}{T}\int_0^T [A(t)]\,dt \;\; ; A = \alpha\,,\,\beta_e\,,\,\beta_f \tag{8}$$

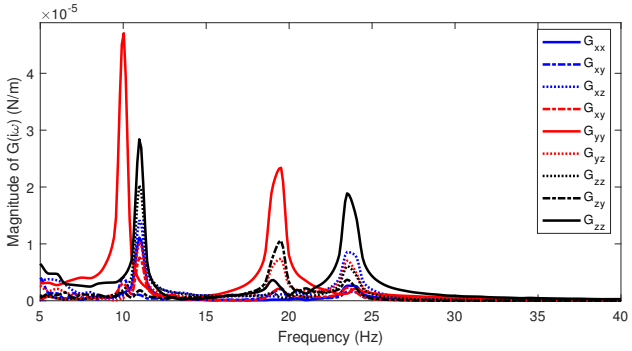

Fig. 3. Measured direct and cross frequency response functions of the KUKA KR 90 robot with joint angles 0°, −70°, 100°, 0°, 0° and 0°, from first to sixth joint, respectively.

In Eq. 7, $\mathbf{X}$ and $\mathbf{X}^\tau$ are the current displacement and delayed displacement vectors, respectively:

$$\begin{aligned}\mathbf{X}(t) &= [x(t) \quad y(t) \quad z(t)]^T\\ \mathbf{X}^\tau(t) &= [x(t-\tau) \quad y(t-\tau) \quad z(t-\tau)]^T\end{aligned} \tag{9}$$

The current and delayed displacement vectors can be mapped to the force vectors using the Frequency Response Function (FRF) matrix $\mathbf{G}$:

$$\begin{aligned}\mathbf{X}(i\omega) &= \mathbf{G}(i\omega)\,\mathbf{F}(i\omega)\\ \mathbf{X}^\tau(i\omega) &= e^{-i\omega\tau}\,\mathbf{G}(i\omega)\,\mathbf{F}(i\omega)\end{aligned} \tag{10}$$

By substituting the deflection terms from Eq. 10, Eq. 7 can be re-written as the following eigenvalue equation:

$$\mathbf{F} = \left\{a_o\,[\alpha_0]\left(1 - e^{-i\omega\tau}\right) - \left([\beta_{e0}] + \lfloor\beta_{f0}\rfloor\right)\right\}\mathbf{GF} \tag{11}$$

The nontrivial solution of the above equation leads to the characteristic equation of the system:

$$\det\left\{\mathbf{I} - \left(a_o\,[\alpha_0]\left(1 - e^{-i\omega\tau}\right) - \left([\beta_{e0}] + \lfloor\beta_{f0}\rfloor\right)\right)\mathbf{G}\right\} = 0 \tag{12}$$

The stability of vibrations at any combination of spindle speed and axial depth of cut is determined by applying Nyquist criterion on the roots of the above characteristic equation [15].

3.2. Case study

A numerical example is presented to study the effect of the feed and edge forces on chatter stability limits. In order to use a realistic representation of the robot flexibility in this example, the direct and cross FRFs of a KUKA KR 90 robotic arm at its wrist are measured using impulse hammer tests. The measured FRFs are shown in Fig. 3. Note that the FRFs at the tool tip, and not the wrist, are to be used in chatter analysis; however, because the available robotic arm did not include a milling end-effector, the FRFs were measured at the wrist to obtain the closest representation of the FRFs at the tool tip.

The stability diagrams are obtained by applying Nyquist criterion on the characteristic equation obtained at each point on a grid of spindle speeds and nominal axial depth of cut a_o. Note that the robot compliance is posture-dependent and can be significantly high in a flexible postures. As shown in Eq. 7, $[\beta_e]$ and

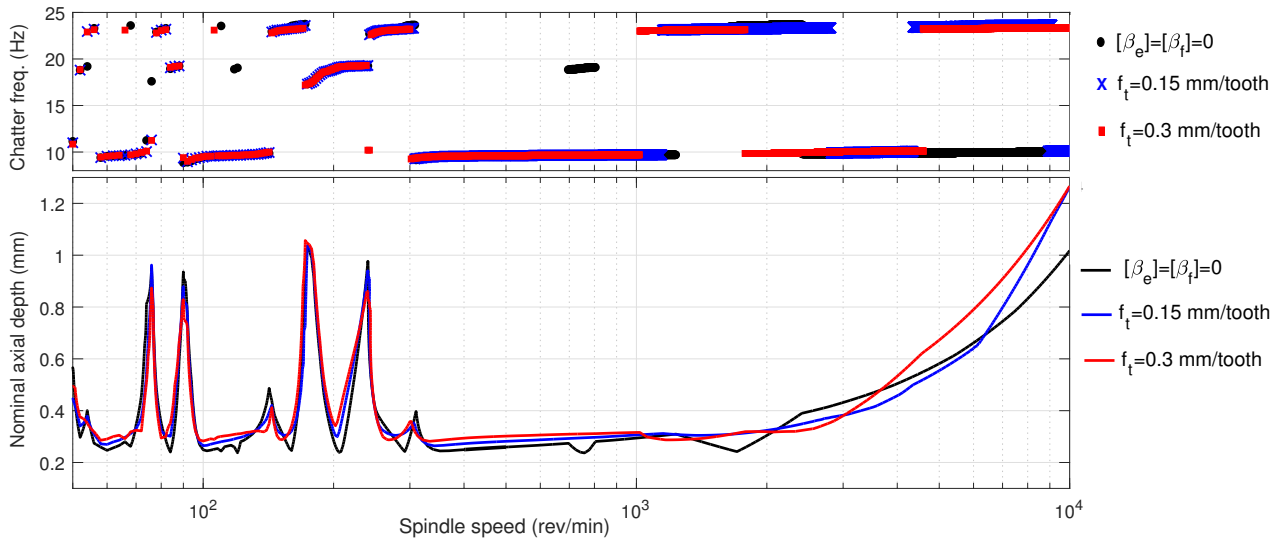

Fig. 4. Stability limit and chatter frequency of half-immersion down milling of Aluminium with KUKA robot; K_{tc} =691 MPa, K_{rc} =263 MPa, K_{ac} =100 MPa, K_{te} =10 N/mm, K_{re} =10 N/mm, K_{ae} =5 N/mm, γ=50° , N =4.

$[\beta_f]$ matrices also act as stiffness matrices and can cause considerable variation in stability limit. The contribution of $[\beta_f]$ to the (un)stability of the system is magnified by increasing feed rate as it proportionally increase by feedrate.

Figure 4 shows the stability diagrams obtained for machining of Aluminum workpiece. As shown in this figure, stability limit at low speed region (< 500rev/min) increases by increasing feedrate. However, the discrepancies between the stability limits with and without the effect of feed and edge forces are even more pronounced at higher cutting speeds. For example, the stability limit at 7000 rev/min increases from 0.74 mm to 0.91 mm for feedrate of 0.3 $mm/tooth$ which corresponds to 22% increase while 17% reduction is observed at 2500 rev/min. Another aspect of the effect of the edge and feed forces on chatter stability can be understood by investigating the chatter frequency shown in Fig. 4. At higher cutting speeds, i.e. approximately above 4000 rev/min, chatter mode shifts from the mode at 10 Hz to the mode around 24 Hz. Figure. 3 shows that the mode at 24Hz is the most flexible in z direction. It can be concluded that by taking into account the effect of axial vibrations on modulation of depth of cut, and consequently on the feed and edge forces, the chatter mode shifts to the mode at 24 Hz.

Stability diagram for low speed milling of Titanium alloy (TiAl6V4) is also shown in Fig. 5. As shown in this figure, the variations of stability limits at lower speeds are more significant. For example, the stability limit around 200 rev/min increases from 0.12 mm to 0.17 mm, a 40% increase in stability limit.

4. Nonlinearity in regenerative forces

The effect of the nonlinear terms that emerge in the regenerative portion of the cutting forces (Eq. 6) is studied by developing numerical simulations in Simulink/MATLAB. The following system of equations is numerically solved to simulate vibrations of the end-effector subjected to nonlinear milling forces:

$$\mathbf{M}\ddot{\mathbf{X}}(t) + \mathbf{C}\dot{\mathbf{X}}(t) + \mathbf{K}\mathbf{X}(t) = \mathbf{F}(t) \tag{13}$$

Because the typical feed speed in robotic machining applications is much slower than cutting speed, the effect of inertial forces (i.e. Coriolis and Centrifugal forces) can be neglected [6, 8, 10, 13].The effect of nonlinear inertial forces is neglected in this simulation as well, and the dynamics of the robot structure is assumed to be linear as described on the left hand side of Eq.13. The matrices $\mathbf{M}$, $\mathbf{C}$ and $\mathbf{K}$ are the mass, damping and stiffness matrices of the robot in Cartesian space. These matrices are obtained from the corresponding matrices in joint space ($\mathbf{M}_q$, $\mathbf{C}_q$ and $\mathbf{K}_q$) using the Jacobian of the robot, $\mathbf{J}$ [16]:

$$\mathbf{M} = \mathbf{J}^{-T}\mathbf{M}_q\mathbf{J}^{-1}\,,\ \mathbf{C} = \mathbf{J}^{-T}\mathbf{C}_q\mathbf{J}^{-1}\,,\ \mathbf{K} = \mathbf{J}^{-T}\mathbf{K}_q\mathbf{J}^{-1} \tag{14}$$

The stiffness and damping matrices in joint space are considered as diagonal matrices of joint stiffness and damping values, respectively. The mass matrix is a function of the inertia of the robot links and joint coordinates [16]. It is assumed that the robot vibrates in a small range of joint angles, so that the robot posture is invariant. Hence, the mass matrix can be considered as a constant matrix.

4.1. Numerical simulation results

Down-milling of Titanium alloy with Staubli TX200 robot is considered. Six degrees of freedom are considered to model the dynamics of the robot as it has six revolute joints. The inertial parameters of the links are derived from the CAD model of the robot to calculate the mass matrix in joint space [16]. Then, the stiffness and damping matrices in joint space are identified in two steps. First, the joint stiffness values are selected such that the square roots of the eigenvalues of $\mathbf{M}_q^{-1}\mathbf{K}_q$ match with

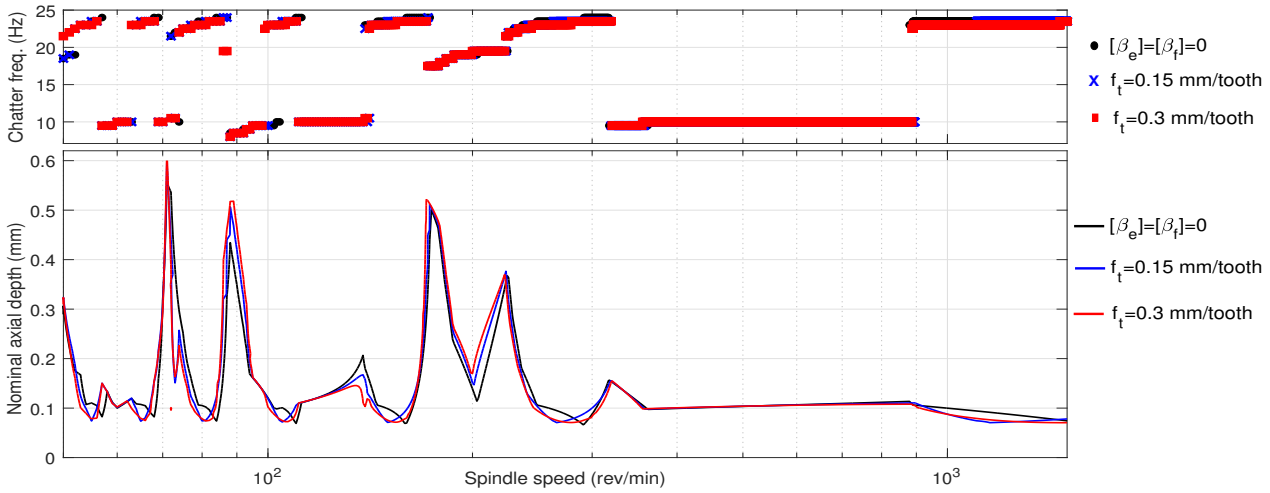

Fig. 5. Stability limit of 20% down milling of Titanium with KUKA robot; K_{tc} =1835 MPa, K_{rc} =1132 MPa, K_{ac} =280 MPa, K_{te} =25 N/mm, K_{re} =45 N/mm, K_{ae} =10 N/mm, γ=41° , N =4.

the measured natural frequencies of the system. The natural frequencies are identified by performing experimental modal analysis. The FRFs are measured using impulse hammer test and the peaks of the measured FRFs are selected as natural frequencies. In the second step, the damping matrix is identified through the comparison of the magnitudes of the measured and simulated FRFs. Since the measured FRFs are defined in Cartesian space, the simulated FRFs need to be calculated in this space as well. Therefore, the identified system matrices in joint space are transformed to the Cartesian space using the relations in Eq. 14. Then, the simulated FRF for a given damping matrix is calculated as follows:

$$\mathbf{G}(\omega) = \left(\mathbf{K} - \mathbf{M}\omega^2 + i\omega\mathbf{C}\right)^{-1} \tag{15}$$

The joint damping values are obtained such that the simulated FRFs using Eq. 15 fit the measured FRFs. Using the full Jacobian matrix, the system matrices in Cartesian space are obtained as follows:

$$\mathbf{M} = \begin{bmatrix} 415.9 & 30.8 & 15.2 & 1.7 & 42.6 & -129.7 \\ 30.8 & 1571 & 330.8 & -17.9 & -0.4 & 2.1 \\ 15.2 & 330.8 & 397.4 & 36.2 & 0.5 & -3.9 \\ 1.7 & -17.9 & 36.2 & 16.6 & 0.3 & -1.7 \\ 42.6 & -0.4 & 0.5 & 0.3 & 22.1 & -56.1 \\ -129.7 & 2.1 & -3.9 & -1.7 & -56.1 & 175.8 \end{bmatrix} (kg)$$

$$\mathbf{K} = \begin{bmatrix} 329.9 & 46.5 & 5.1 & 0.2 & 193.2 & 435 \\ 46.5 & 2895 & 281.8 & -182.3 & -0.2 & 7.8 \\ 5.1 & 281.8 & 345.8 & 108.2 & -2 & 0.01 \\ 0.2 & -182.3 & 108.2 & 124.8 & 1.3 & -6.3 \\ 193.2 & -0.2 & -2 & 1.3 & 197.4 & -351.4 \\ 435 & 7.8 & 0.01 & -6.3 & -351.4 & 778 \end{bmatrix} \times 10^4 (N/m)$$

$$\mathbf{C} = \begin{bmatrix} 4713 & 134 & 20 & 17 & 2004 & 4616 \\ 134 & 12075 & 1147 & -1061 & -17 & 83 \\ 20 & 1147 & 1716 & 696 & 12 & 0.1 \\ 17 & -1061 & 696 & 12 & 19 & -63 \\ 2004 & -17 & 12 & 19 & 1978 & -3527 \\ 4616 & 83 & 0.1 & -63 & -3527 & 7830 \end{bmatrix} (N.s/m)$$

The simulated FRFs are presented in Fig. 6. Note that substituting the above 6×6 system matrices into Eq. 15 results in a 6×6 transfer function matrix which includes FRFs between

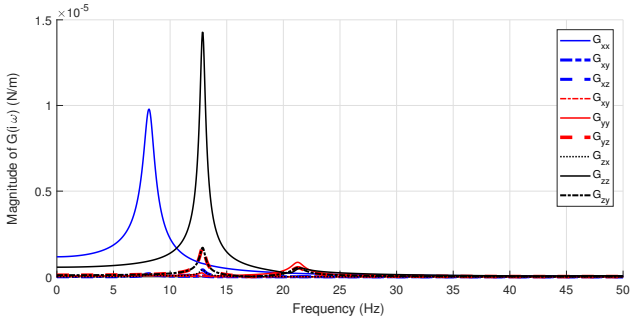

Fig. 6. Simulated direct and cross FRFs of the Staubli TX200 robot.

torques and angular displacements as well. In Fig. 6, only the force-displacement FRFs are shown. Assuming 20% radial immersion down milling using a 4-tooth milling tool, stability lobe diagrams without considering the nonlinear term is constructed using the method described in Section 3.1 and FRFs shown in Fig. 6. The resulting diagram is presented in Fig. 7. As it can be

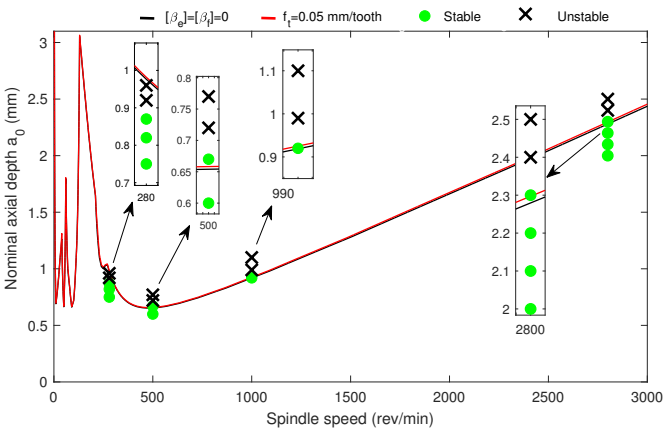

Fig. 7. Stability limit of 20% down milling of Titanium with Staubli robot; K_{tc} =1835 MPa, K_{rc} =1132 MPa, K_{ac} =280 MPa, K_{te} =25 N/mm, K_{re} =45 N/mm, K_{ae} =10 N/mm, γ=50° , N =4.

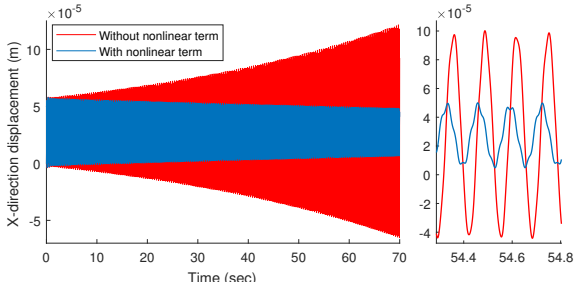

Fig. 8. Stabilizing effect of the nonlinear term in cutting forces at spindle speed of 500 *rev*/*min* and cutting conditions given in Fig. 7.

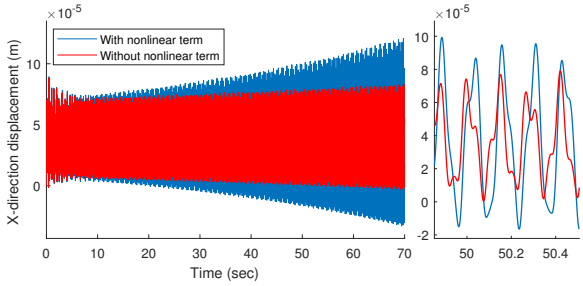

Fig. 9. Destabilizing effect of the nonlinear term in cutting forces at spindle speed of 280 *rev*/*min* and cutting conditions given in Fig. 7.

seen in this figure, the effect of feed and edge forces are negligible in this case, due to low values of feed rate (0.05 *mm*/*tooth*) and edge force coefficients. The end-effector vibrations are simulated considering the nonlinear term by numerically solving Eq. 13 at different spindle speeds and nominal axial depth of cuts. Stable vibrations are shown with green circles while the black cross marks stand for unstable vibrations.

As shown in Fig. 7, the nonlinear term of cutting forces can have both stabilizing and destabilizing effects at different spindle speeds. For example, at spindle speed of 500 *rev*/*min*, the stability limit increases from 0.66 *mm* to 0.70 *mm*, which is about 6% increase in stability limit, while 9% reduction is observed at 280 *rev*/*min*. Figure 8 shows the simulated vibrations in X-direction of the end-effector when subjected to linear and nonlinear cutting forces at 0.67 *mm* nominal depth of cut. The system is unstable if the nonlinear terms are neglected and the vibration amplitude grows with time. The nonlinear term has damping effect and stabilizes the system. Similar stabilizing effect has been observed at 1000 *rev*/*min* and 2800 *rev*/*min*. However, the amplitude of simulated vibrations increases when considering the nonlinear term at spindle speed of 280 *rev*/*min* and nominal cutting depth of 0.92 *mm*; as shown in Fig. 9.

5. Conclusions

The effect of depth of cut modulation due to axial vibrations in robotic milling was investigated. It was shown that the modulation of depth of cut leads to additional stiffness-like terms in the equation of chatter. These terms arise from the edge and feed-generated forces. In addition, nonlinearities emerge in the regenerative cutting forces model. The effect of edge and feed-generated forces as well as nonlinear regenerative terms on the vibrations stability during robotic milling was studied using numerical examples. Both of the additional stiffness-like and nonlinear terms were shown to have significant effect on stability of the process, particularly when the robot is in its flexible posture.

Acknowledgements

The authors would like to thank Mr. Hoai Nam Huynh and the department of Theoretical Mechanics, Dynamics and Vibrations of University of Mons for providing experimental data of Staubli TX200 Robot. This project was financially supported by the Natural Sciences and Engineering Research Council of Canada under Discovery Grant program.

References

[1] Chen, Y. and Dong, F., 2013. Robot machining: recent development and future research issues. The International Journal of Advanced Manufacturing Technology, 66(9-12), pp.1489-1497.
[2] Iglesias, I., Sebastin, M.A. and Ares, J.E., 2015. Overview of the state of robotic machining: Current situation and future potential. Procedia engineering, 132, pp.911-917.
[3] Lehmann, C., Pellicciari, M., Drust, M. and Gunnink, J.W., 2013. Machining with industrial robots: the COMET project approach. In Robotics in Smart Manufacturing (pp. 27-36). Springer, Berlin, Heidelberg.
[4] Schneider U, Ansaloni M, Drust M, Leali F, Verl A. Experimental investigation of sources of error in robot machining. InRobotics in Smart Manufacturing 2013 (pp. 14-26). Springer, Berlin, Heidelberg.
[5] Quintana, G. and Ciurana, J., 2011. Chatter in machining processes: A review. International Journal of Machine Tools and Manufacture, 51(5), pp.363-376.
[6] Wang, J., Zhang, H. and Pan, Z., 2006. Machining with flexible manipulators: Critical issues and solutions. In Industrial Robotics: Programming, Simulation and Applications. InTech.
[7] Gasparetto, A., 1998. A system theory approach to mode coupling chatter in machining. Journal of dynamic systems, measurement, and control, 120(4), pp.545-547.
[8] Cen, L. and Melkote, S.N., 2017. CCT-based mode coupling chatter avoidance in robotic milling. Journal of Manufacturing Processes, 29, pp.50-61.
[9] Huynh, H.N., Rivire-Lorphvre, E. and Verlinden, O., 2016, May. Integration of machining simulation within a multibody framework: application to milling. In IMSD: The 4th Joint International Conference on Multibody System Dynamics.
[10] Mousavi, S., Gagnol, V., Bouzgarrou, B.C. and Ray, P., 2017. Dynamic modeling and stability prediction in robotic machining. The International Journal of Advanced Manufacturing Technology, 88(9-12), pp.3053-3065.
[11] Budak, E. and Altintas, Y., 1998. Analytical prediction of chatter stability in millingpart I: general formulation. Journal of dynamic systems, measurement, and control, 120(1), pp.22-30.
[12] Altintas, Y., 2012. Manufacturing automation: metal cutting mechanics, machine tool vibrations, and CNC design. Cambridge university press.
[13] Cordes, M., Hintze, W., Altintas, Y. 2019. Chatter stability in robotic milling. In Robotics and Computer-Integrated Manufacturing, Volume 55, p. 11-18.
[14] Insperger T, Stpn G. Semidiscretization method for delayed systems. International Journal for numerical methods in engineering. 2002 Oct 20;55(5):503-18.
[15] Eynian, M., 2010. Chatter stability of turning and milling with process damping (Doctoral dissertation, University of British Columbia).
[16] Siciliano, B. and Khatib, O. eds., 2016. Springer handbook of robotics. Springer.